TOMOGRAPHY® RESEARCH ARTICLE

Cubic-Spline Interpolation for Sparse-View CT Image Reconstruction With Filtered Backprojection in Dynamic Myocardial Perfusion Imaging

Esmaeil Enjilela[1], Ting-Yim Lee[1,2], Gerald Wisenberg[3], Patrick Teefy[3], Rodrigo Bagur[3], Ali Islam[4], Jiang Hsieh[5], and Aaron So[1,2]

[1]Imaging Research Laboratories, Robarts Research Institute, University of Western Ontario, London, ON, Canada; [2]Imaging Program, Lawson Health Research Institute, London, ON, Canada; [3]Department of Cardiology, London Health Sciences Centre, London, ON, Canada; [4]Department of Radiology, St. Joseph's Healthcare London, London, ON, Canada; and [5]Department of Molecular Imaging & Computed Tomography, GE Healthcare, Waukesha WI

Corresponding Author:
Aaron So, PhD
Department of Imaging, Lawson Health Research Institute, 268 Grosvenor Street, London, ON, Canada, N6A 4V2;
E-mail: aso@robarts.ca

Key Words: myocardial perfusion, sparse-view image reconstruction, filtered backprojection, projection interpolation, cubic spline, radiation dose reduction.
Abbreviations: Dynamic contrast-enhanced (DCE), filtered backprojecton (FBP), computed tomography (CT), myocardial perfusion (MP)

ABSTRACT

We investigated a projection interpolation method for reconstructing dynamic contrast-enhanced (DCE) heart images from undersampled x-ray projections with filtered backprojecton (FBP). This method may facilitate the application of sparse-view dynamic acquisition for ultralow-dose quantitative computed tomography (CT) myocardial perfusion (MP) imaging. We conducted CT perfusion studies on 5 pigs with a standard full-view acquisition protocol (984 projections). We reconstructed DCE heart images with FBP from all and a quarter of the measured projections evenly distributed over 360°. We interpolated the sparse-view (quarter) projections to a full-view setting using a cubic-spline interpolation method before applying FBP to reconstruct the DCE heart images (synthesized full-view). To generate MP maps, we used 3 sets of DCE heart images, and compared mean MP values and biases among the 3 protocols. Compared with synthesized full-view DCE images, sparse-view DCE images were more affected by streak artifacts arising from projection undersampling. Relative to the full-view protocol, mean bias in MP measurement associated with the sparse-view protocol was 10.0 mL/min/100 g (95%CI: −8.9 to 28.9), which was >3 times higher than that associated with the synthesized full-view protocol (3.3 mL/min/100 g, 95% CI: −6.7 to 13.2). The cubic-spline-view interpolation method improved MP measurement from DCE heart images reconstructed from only a quarter of the full projection set. This method can be used with the industry-standard FBP algorithm to reconstruct DCE images of the heart, and it can reduce the radiation dose of a whole-heart quantitative CT MP study to <2 mSv (at 8-cm coverage).

INTRODUCTION

Computed tomography (CT) myocardial perfusion (MP) imaging is a technique used to quantitatively measure myocardial blood flow (perfusion) through tracer kinetic modeling of the time-enhancement curves acquired from dynamic contrast-enhanced (DCE) CT scanning of the heart. As this technique requires repeated scanning of the heart following a short bolus injection of contrast solution, the associated radiation dose is higher than that required for a standard chest CT scan. A straightforward strategy to minimize radiation exposure is to lower the tube current setting (measured in milliampere or mA) for dynamic scanning, and that to correct for excessive projection noise is to use postprocessing techniques such as highly constrained back-projection local reconstruction (HYPR-LR) (1-3), multiband filtering (4), sinogram smoothing (5), or statistics-based iterative reconstruction (6, 7). However, there are 2 main challenges associated with the ultralow-milliampere approach. First, photon starvation could lead to inaccurate sampling of the arterial and myocardial time-enhancement curves and sequentially the measurement of MP. Second, the CT detector electronic noise becomes dominant at the extremely low milliampere level, which is difficult to model and correct for with Poisson statistics alone.

Sparse-view dynamic acquisition, where only a small number of x-ray projections are acquired in each gantry rotation, is an alternative solution to achieve ultralow-dose CT MP imaging.

ISSN 2379-1381 https://doi.org/10.18383/j.tom.2019.00013

This approach is not restricted by the electronic noise barrier and hence could achieve more dose reduction than the low-milliampere approach. Furthermore, the feasibility of the sparse-view acquisition with a clinical CT scanner capable of rapid x-ray pulsing has been demonstrated (8). However, sparse-view acquisition can induce aliasing streak artifacts in the reconstructed images (9, 10), which could have a significant impact on the measurements of time-enhancement curves and MP.

In this paper, we investigated whether reconstruction of streak-free DCE heart images from undersampled projections by using the standard filtered backprojection (FBP) algorithm is feasible if the missing projections are estimated from neighboring ones. The performance of this view interpolation method was evaluated in CT MP studies of pigs, in which a subset of measured projections was used to generate DCE heart images and MP maps with and without the view interpolation applied, and the image quality and MP measurement against the reference full-view technique were compared.

METHODS AND MATERIALS

Animal Model

DCE-CT imaging was performed on 5 farm pigs that weighed 40–50 kg. The animal studies were approved by the institutional animal research ethics review board. Two pigs had acute myocardial infarction induced in the apical wall of the left ventricular myocardium from a transient occlusion of the distal left anterior descending (LAD) artery with a balloon catheter for 1 h followed by reperfusion. The other 3 pigs were normal and without infarction. These pigs collectively provided a wide spectrum of myocardial tissue, from normal to abnormal (ischemic or infarcted), for the validation of the cubic-spline-view interpolation method for the sparse-view image reconstruction with FBP.

Projection Data Acquisition

In each CT MP study, the pig was intubated and mechanically ventilated, and they were placed in either a supine or lateral position on the CT scanner table. Before each DCE-CT acquisition, iodinated contrast solution (Iohexol 300 mgI/mL) was injected into a peripheral vein at 3 mL/s and at a dosage of 0.7 mL/kg body weight, followed by saline flush at the same injection rate. The ventilator was turned off to minimize breathing motion during the short acquisition (~30 s). Using a 64-row CT750 HD scanner (GE Healthcare, Waukesha, WI) operating in a prospective electrocardiogram-gated acquisition mode, a 4-cm section of the heart covering the largest cross-section of the left ventricle in the axial tomographic plane was scanned at 3–4 s after contrast injection over 20–25 heart beats at mid-diastole. For each full (360°) gantry rotation at 140-kV tube voltage, 80-mA tube current, 8- × 5-mm collimation width, and 0.35-s gantry rotation period, the full-view projection set consisted of 984 projections. From each full-view projection set, 1 out of every 4 consecutive projections was selected to generate the sparse-view set of 246 projections distributed evenly over 360°.

Image Reconstruction

For each pig, the following 3 sets of DCE heart images were reconstructed from the 3 projection sets with FBP: (a) full-view (984 views), (b) sparse-view (246 views), and (c) synthesized full-view (984 views). The synthesized full-view projection set was generated by applying a cubic-spline interpolation of the sparse-view projection set in (b).

Different algorithms are available to generate missing projections from a discrete set of sampled projections. Generally speaking, with n measured data points, a single $(n-1)^{\text{th}}$ order polynomial can be used for the interpolation. Although polynomial interpolation is a common choice of interpolants, the associated error of interpolation can be large when a high-order polynomial function is used for data fitting. Such an interpolation error can be minimized by using spline interpolation which applies low-order polynomials to subsets of data points (11). Let us denote $f(x)$ as a function between the sampled data points, x_{i-1} and x_i, with $i = [1, \ldots, n]$. A spline $S(x)$ is a piecewise (composite) function formed by n low-order polynomials $P(x)$ each fitting $f(x)$.

$$S(x) = \begin{cases} P_1(x) \\ \vdots \\ P_i(x) \\ \vdots \\ P_n(x) \end{cases} \tag{1}$$

Compared with a single high-order polynomial function, spline interpolation should provide a more accurate approximation of $f(x)$, particularly if there exists local abrupt changes (such as the edges between high- and low-contrast regions). A cubic spline is a spline constructed of piecewise third-order polynomials (12, 13). Let us consider 3 consecutive data points, namely, x_{i-1}, x_i, x_{i+1}. Mathematically, a third-order polynomial $P(x)$ on the interval between data points x_{i-1} and x_i can be expressed as follows:

$$P_i(x) = a_i + b_i x + c_i x^2 + d_i x^3 \tag{2}$$

where a_i, b_i, c_i, and d_i are coefficients, and $1 \le i < n$. Similarly, the third-order polynomial between data points x_i and x_{i+1} has the following form:

$$P_{i+1}(x) = a_{i+1} + b_{i+1} x + c_{i+1} x^2 + d_{i+1} x^3 \tag{3}$$

The polynomials in equations (2) and (3) at their connecting data point (x_i) should be identical so that $S(x)$ is continuous:

$$P_i(x_i) = P_{i+1}(x_i) = f(x_i) \tag{4}$$

In addition, the derivatives of the polynomials should be identical at x_i for $S(x)$ to be smooth. For instance:

$$P_i'(x_i) = P_{i+1}'(x_i); \quad P_i''(x_i) = P_{i+1}''(x_i) \tag{5}$$

Solving the above equations yield $n-1$ equations with $n+1$ unknowns. The assumption of boundary conditions can be made to obtain 2 additional equations that are required to solve for all the unknowns. Conventionally, we can assume the first and second derivatives at the end points x_0 and x_n, respectively, are zero:

$$P_i'(x_0) = P_i'(x_n) = 0; \quad P_i''(x_0) = P_i''(x_n) = 0 \tag{6}$$

The cubic-spline interpolation is based on the least squares method with the cubic convolution interpolation function (12, 13). Taking equations (1) to equations (6) into account, the

cubic-spline interpolation function $I(x)$ can be expressed as follows (14):

$$I(x) = \sum_i c_i s\left(\frac{x - x_i}{h}\right) \quad (7)$$

where x_i are the interpolation nodes, S is the spline interpolation kernel as defined above, h is the sampling interval, and c_i is selected so that the interpolation function is continuous. Cubic-spline interpolation of the measured projections was implemented using Matlab.

Image Analysis

Comparison of MP measurement. The 3 sets of DCE heart images of each pig were analyzed with the CT Perfusion software (GE Healthcare, Waukesha, Wisconsin) to generate MP maps with a model-based deconvolution algorithm (15). The mean MP value in the lateral, apical, and septal walls of the left ventricular myocardium in the axial view over 8 consecutive 5-mm slices were compared between the 3 image reconstruction schemes. In total, 120 ischemic and nonischemic myocardial segments from 5 pigs were available for comparison. Bland–Altman graphical analysis was used to determine the mean bias of the sparse-view and synthesized full-view MP measurements with respect to that of the reference full-view MP measurements. The limits of agreement were presented as 95% confidence intervals.

Comparison of Image Difference. We used an image difference metric described by Busono and Hussein (16) to determine which between the sparse-view and the synthesized full-view FBP reconstruction produced DCE heart images best matched with images from the full-view FBP reconstruction. The image difference at time point t, δ^t_{Dif}, is defined as follows:

$$\delta^t_{Dif} = \frac{\|I^t_{Rec} - I^t_{FV}\|}{\|I^t_{FV}\|} \times 100 \quad (8)$$

where I^t_{Rec} is the image at time t reconstructed with FBP from either the 246-view or synthesized 984-view projection set; I^t_{FV} is the reference full-view FBP image at time t; and $\|\cdot\|$ denotes the Euclidean norm.

RESULTS

Figure 1A shows the sinogram of a full-view projection set acquired at one slice location. This full-view sinogram was then subsampled to generate a sparse-view set of 246 projections evenly distributed over 360° as shown in Figure 1B. The dark vertical lines in Figure 1B are projections in the full-view set that were left out in the sparse-view set. The sinogram of the corresponding synthesized full-view projection set is shown in Figure 1C for comparison. The 2 sinograms in Figure 1, A and C were qualitatively similar to each other. For a more quantitative comparison, Figure 1D shows the projection profile of the full-view sinogram (solid black line) superimposed over the projection profile of the synthesized (interpolated) full-view sinogram (dashed blue line) at the central detector for one slice location. The 2 projection profiles were comparable to each other, with the profile from the synthesized full-view sinogram slightly smoother than that from the measured full-view sinogram. For reference, the red stars in Figure 1D denote the corresponding projection profile of the sparse-view sinogram.

Figure 2 shows the DCE heart images reconstructed from the full-view (Figure 2, A and B), sparse-view (Figure 2, C and D) and synthesized full-view (Figure 2, E and F) projection sets. Image reconstruction with the sparse-view projection set resulted in streak artifacts. Figure 2, G and H show the difference image between the full-view (Figure 2A) and sparse-view (Figure 2C) protocols and that between the full-view (Figure 2A) and synthesized full-view (Figure 2E) protocols, respectively. The mean ± standard deviation of CT number in 3 different regions in Figure 2G (lateral wall and apical wall of the left ventricular myocardium and a peripheral soft tissue region) was 8.74 ± 12.71, 10.69 ± 13.84, and 10.14 ± 15.20 Hounsfield unit (HU), which was larger than that of CT number in the 3 different regions in Figure 2H (5.28 ± 8.34, 5.88 ± 8.82, and 7.06 ± 9.32 HU), suggesting that the cubic-spline interpolation method was able to reduce the HU errors in the reconstructed images arising from aliasing streak artifacts. As shown in Figure 2I, the image difference metric [equation (8)] between the synthesized full-view and full-view DCE images was consistently <4% at all time points, in comparison to 7.5% between the sparse-view and the full-view DCE images.

Figure 3 shows the MP maps of a pig with an infarct in the apical myocardium (yellow arrow), derived from the 3 sets of DCE images shown in Figure 2. The MP map generated from the sparse-view images (Figure 3B) was clearly noisier than that generated from the full-view images (Figure 3A). After cubic-spline view interpolation was applied, the MP map generated from the synthesized full-view images (Figure 3C) was comparable with that generated from the full-view images (Figure 3A).

The Bland–Altman plot shown in Figure 4 showed that the mean bias of absolute MP measurement associated with the synthesized full-view and sparse-view protocols was 3.6 (95% CI −8.6 to 15.7) mL/min/100 g and 9.7 (95% CI −12.8 to 32.3) mL/min/100 g, respectively, with respect to the reference full-view protocol. Furthermore, the cubic-spline interpolation method led to a 63% decrease in the mean bias of absolute MP measurement when the sparse-view DCE heart images were used for perfusion analysis.

DISCUSSION

Quantitative CT MP imaging is useful for the functional assessment of coronary artery disease (17) but high radiation dose is a major hurdle for its implementation in routine clinical practice. This study aimed to demonstrate the feasibility of reducing the radiation dose of a quantitative CT MP study with the sparse-view dynamic acquisition and image reconstruction. CT image reconstruction with sparsely sampled projections has been of great interest lately. Although compressed sensing is the primary algorithmic choice for sparse-view CT image reconstruction with promising results reported in a number of preclinical studies (18, 19), it can lead to loss of image details in aspects of contrast and spatial resolution. Although more advanced compressed sensing–based algorithms have been recently developed to improve these aspects (20-22), they remain computationally demanding, which may limit their clinical applications. In contrast, FBP-based image reconstruction methods are faster, making the sparse-view CT MP imaging more feasible in real-world clinical settings.

To the best of our knowledge, the application of cubic-spline interpolation for sparse-view CT MP measurement has

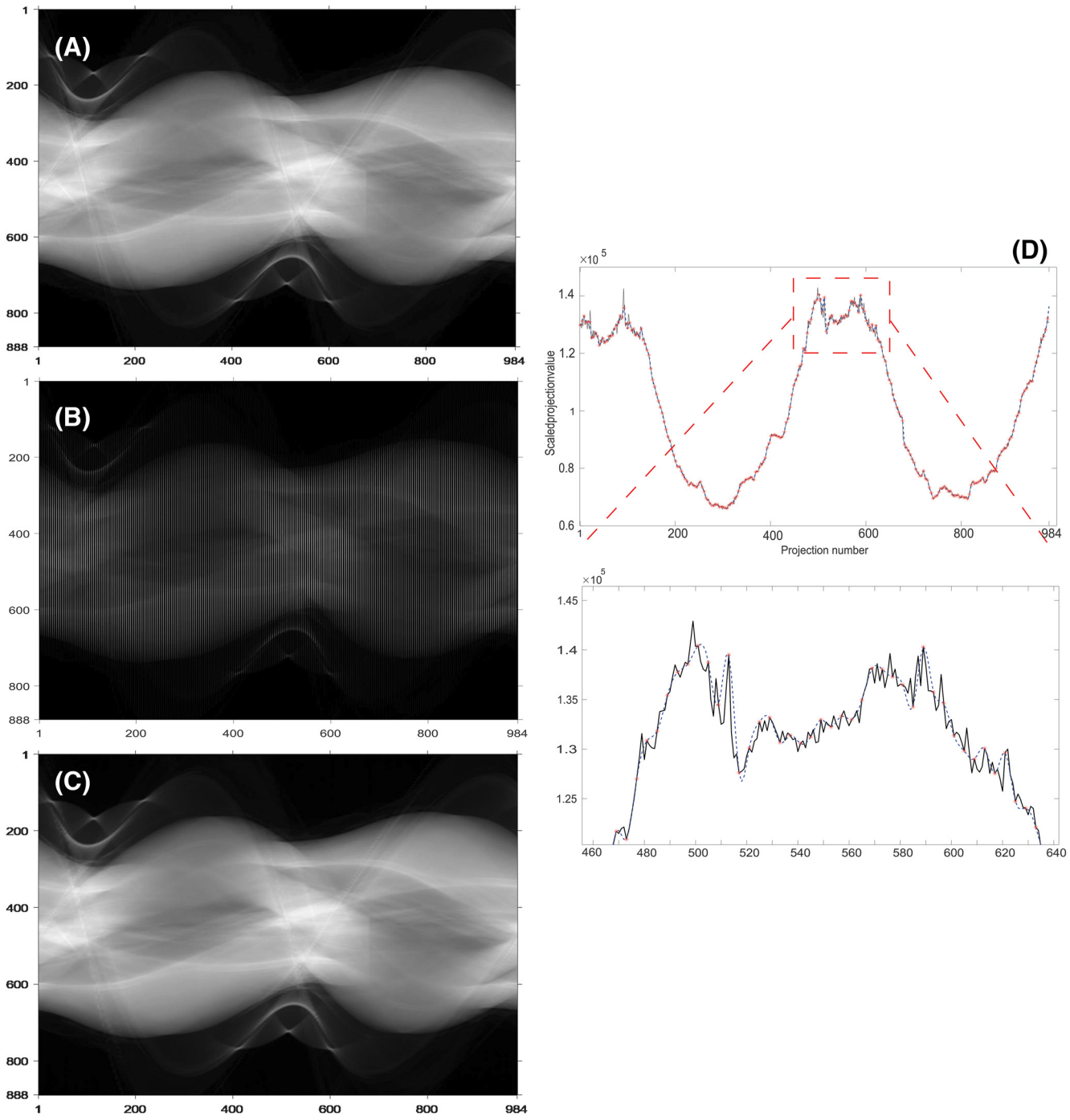

Figure 1. Sinograms of a pig computed tomography (CT) myocardial perfusion (MP) study acquired with the full 984-view (A), sparse 246-view (B), and synthesized full 984-view protocols (C). The *y*- and *x*-axis represent the detector and projection numbers, respectively. Projection profile of the full-view sinogram is compared with that of the synthesized full-view sinogram at the central detector (D). The red star marks the evenly subsampled 246 views from the full-view projection set.

not been previously investigated. The main challenge of this approach is the aliasing streak artifacts in reconstructed DCE images that can significantly affect the accuracy of MP measurement. A cubic-spline interpolation method was used in our studies conducted in pigs to estimate the missing projections before FBP image reconstruction to minimize the aliasing streak artifacts in DCE images. Our findings showed that the number of projections required for reconstructing relatively streak-free DCE heart images with the conventional FBP algorithm could be reduced to 25% of the full-view projection set (from 984 to 246 views), as evident by the subtle image difference with respect to the reference full-view protocol

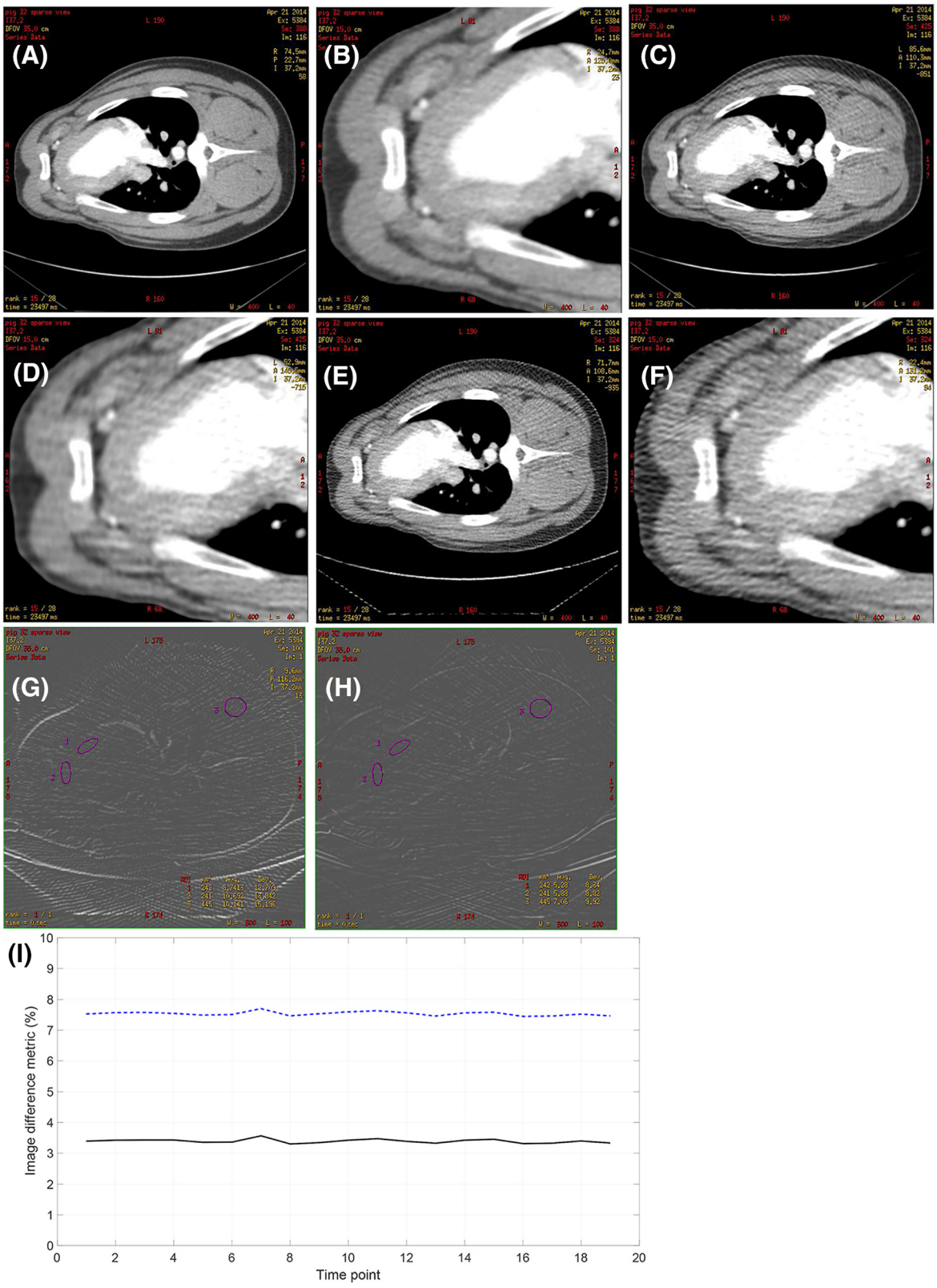

Figure 2. Contrast-enhanced CT images from a pig heart reconstructed with filtered backprojecton (FBP) from full-view(A, B), sparse-view (C, D), and synthesized full-view projections (E, F). These images corresponded to the time when both heart chambers were filled with an iodinated contrast solution. The window width/level was set at 400/40 HU. (G) and (H) depict the difference images between (A) and (C) and between (A) and (E), respectively. Image difference metric for synthesized full-view images (black solid line) is compared with that for sparse-view images (dashed blue line) over the whole time course of a dynamic CT MP study (I).

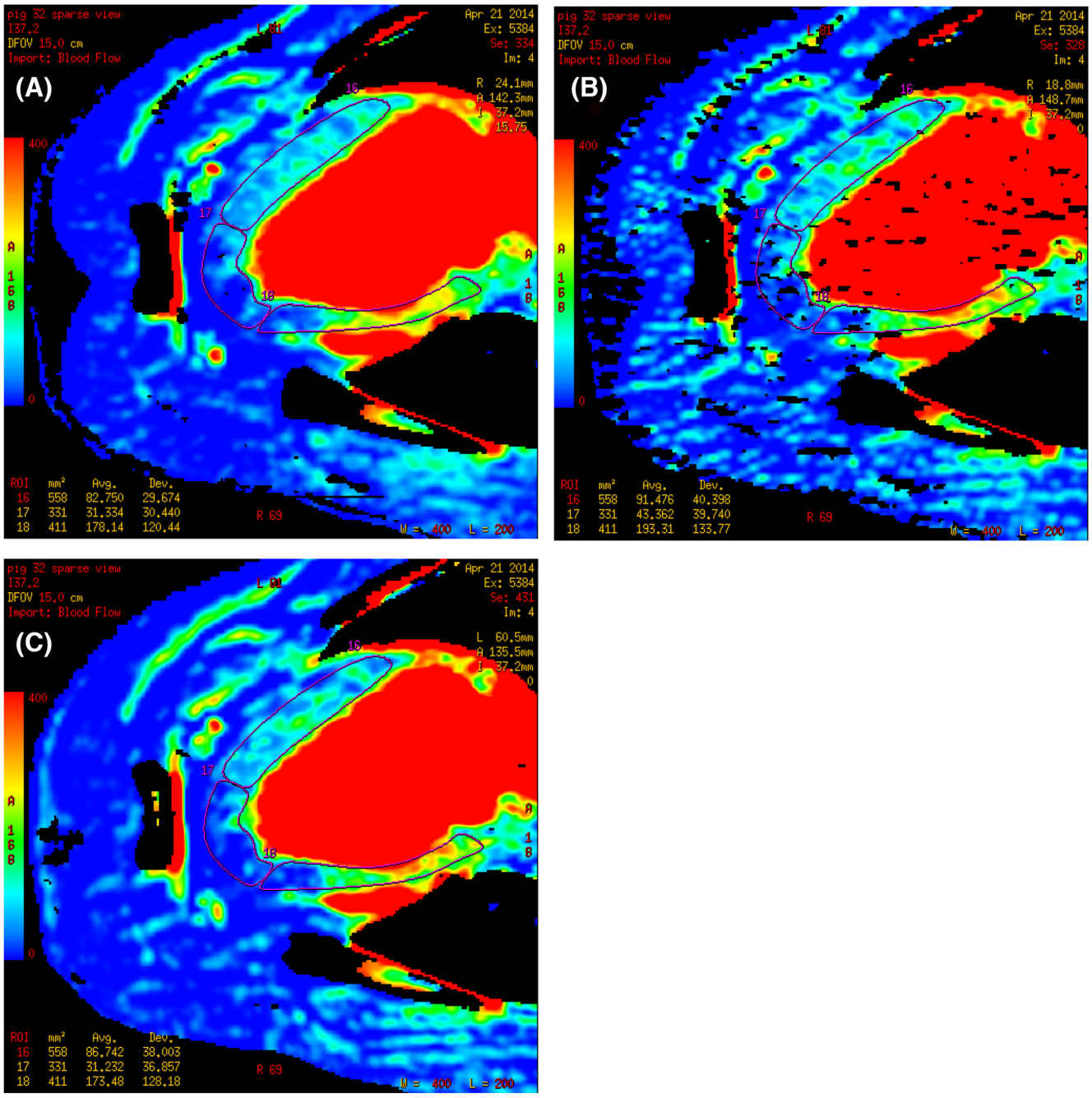

Figure 3. CT MP maps derived from dynamic contrast-enhanced (DCE) images reconstructed from full-view (A), sparse-view (B), and synthesized full-view (C) projections with FBP as shown in Figure 2. The CT MP maps are displayed in a color scale range from 0 (blue) to 400 (red) mL/min/100 g. The yellow arrow in (A) points to the infarcted region within the apical wall of the myocardium.

(<4% for all time points, Figure 2I). The accuracy of MP measurement was also minimally affected, as reflected by the small bias in MP measurement with respect to the full-view protocol (<4 mL/min/100 g; Figure 4B). Without view interpolation, the corresponding image difference and bias in MP measurement were 2 and 3 times higher, respectively.

The effective dose of a quantitative CT MP study covering 8 cm of the heart with the full-view dynamic acquisition protocol, estimated from the dose-length product reported on the scanner, was 8 mSv. With a 4-fold reduction in projection views (from 984 to 246), the effective dose of the sparse-view dynamic acquisition protocol was reduced to 2 mSv.

The same magnitude of radiation dose reduction can be achieved by reducing the x-ray tube current from 80 mA to 20 mA while keeping all the projection views (984). However, such an approach leads to much poorer signal-to-noise ratio in each

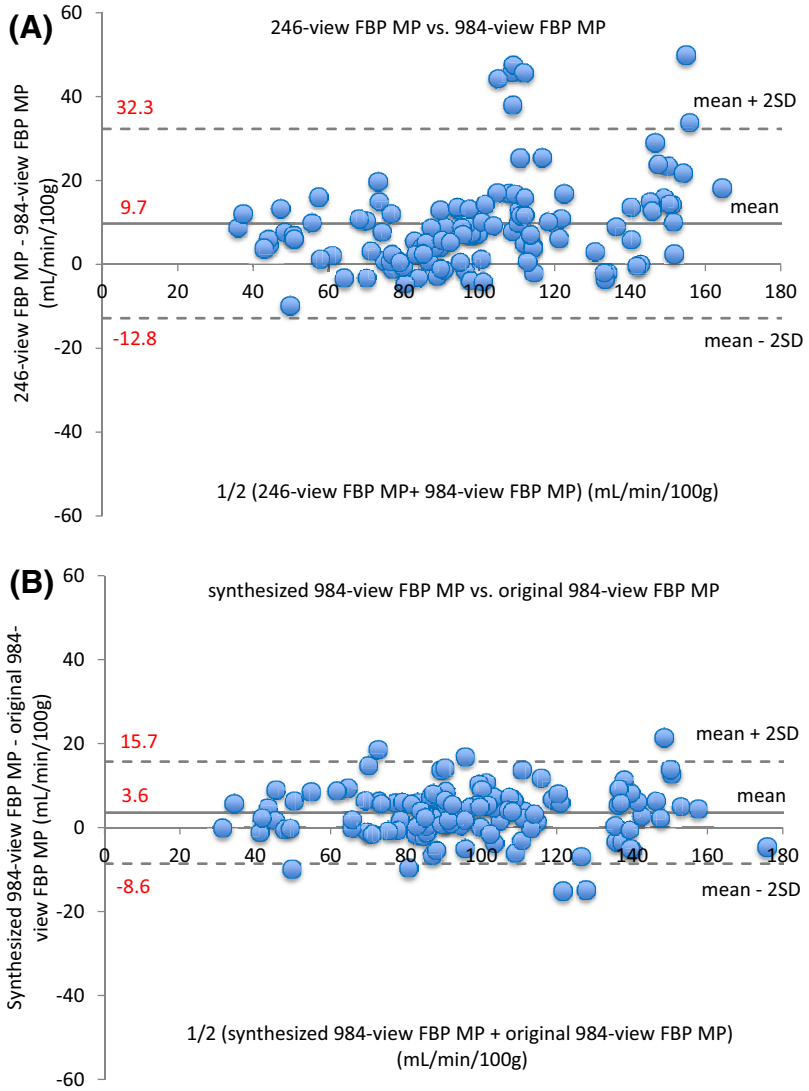

Figure 4. (A) Sparse-view and (B) synthesized full-view CT MP measurements in comparison to the reference full-view MP measurements using the Bland–Altman graphical analysis. The solid gray line in each graph represents the mean bias in MP measurement relative to the reference protocol. The dotted gray lines denotes the 95% confidence intervals (CIs) of the estimated mean bias. The numbers in red color in each graph represent the mean bias and corresponding CI values of MP.

measured projection, and the system electronic noise may exert a greater impact at low mA which is difficult to correct for with Poisson statistics. By contrast, the signal-to-noise ratio of each measured projection in the sparse-view dynamic acquisition is maintained. As such, the sparse-view acquisition may be a better option for radiation dose reduction than low-milliampere acquisition in this regard.

It is noteworthy to mention that the use of interpolated projection views introduced the blurring of sharp edges in the reconstructed DCE heart images, as depicted in Figure 2, E and F. However, extremely high spatial resolution is not necessary for CT MP imaging, as MP maps are typically generated with one-half of the spatial resolution of the source images. The noise in the synthesized full-view images was also lower than the full-view images and was contributed by the low-pass filtering effect inherent to interpolation.

In addition to the cubic-spline interpolation applied in our studies, other advanced algorithms such as directional sinogram interpolation (23, 24) and deep-learning-based interpolation (25) have been recently developed for generating additional projections to minimize streak artifacts in the sparse-view CT image reconstruction. In the directional sinogram interpolation, the measured projections are first combined to generate the sinogram, which is then downsized with a specialized filter along the axis in parallel to the plane of gantry rotation. The purpose of sinogram downsizing is to eliminate the disconnected traces of the sinogram as a result of sparse-view acquisition before the calculation of the structure tensor. Weighted pixel interpolation is then performed after estimation of the sinogram orientation. The entire interpolation process can be executed iteratively to generate more projections to further minimize the streak artifacts (24). In the deep-learning-based interpolation, the sinogram sampled from the sparse-view acquisition is first up-sampled with a linear interpolation. Then, a synthesized sinogram with quality superior to the linearly interpolated sinogram is generated with a pretrained convolution neural network followed by image reconstruction (25). Preliminary results have suggested that both the directional sinogram interpolation and the deep-learning-based interpolation are promising to generate streak-free CT images from the sparse-view acquisition. Further research should focus on comparing the image quality (such as contrast and spatial resolution) and computation efficiency among different projection interpolation methods available for the sparse-view CT image reconstruction in dynamic perfusion imaging.

The cubic-spline view interpolation method allows the standard FBP algorithm to be used for sparse-view image reconstruction without the need of implementing iterative reconstruction algorithms such as compressed sensing, which is more computationally demanding. Moreover, our previous studies revealed that the minimum number of projections required to produce streak-free DCE heart images with compressed sensing was 328 (26). In comparison, the cubic-spline view interpolation method permits FBP image reconstruction with merely 246 views, which results in a greater degree of dose reduction for quantitative CT MP imaging.

CONCLUSION

The findings of this study suggest that ultra-low-dose quantitative CT MP measurement can be attained with sparse-view dynamic contrast-enhanced acquisition, provided the missing projections can be properly estimated using a cubic-spline interpolation method before image reconstruction. The number of projections required for generating the DCE heart images can be reduced to just 25% of the conventional full-view setting without affecting the absolute MP measurements. The cubic-spline interpolation method allows the conventional FBP algorithm to be used for the sparse-view image reconstruction in CT MP imaging, avoiding the need of implementing the more computationally demanding algorithms such as compressed sensing. The substantial reduction in radiation exposure associated with the sparse-view dynamic acquisition may lead to a wider clinical application of quantitative CT MP imaging for functional assessment of coronary artery disease.

ACKNOWLEDGMENTS

We sincerely thank Jennifer Hadway, Laura Morrison, Dave Gaskin, and Anna MacDonald from Lawson Health Research Institute and St. Joseph's Healthcare London for assisting the animal imaging studies. The project was funded by the Natural Sciences and Engineering Research Council of Canada (NSERC) Discovery Grant.

Disclosures: No disclosures to report.

Conflict of Interest: The authors have no conflict of interest to declare.

REFERENCES

1. Johnson KM, Velikina J, Wu Y, Kecskemeti S, Wieben O, Mistretta CA. Improved waveform fidelity using local HYPR reconstruction (HYPR LR). Magn Reson Med. 2008;59:456–462.
2. Liu X, Primak AN, Krier JD, Yu L, Lerman LO, McCollough CH. Accurate, in vivo determination of renal perfusion and hemodynamics using a ten-fold decrease in radiation dose and HYPR noise reduction. Radiology. 2009;253:98–105.
3. Supanich M, Tao Y, Nett B, Pulfer K, Hsieh J, Turski P, Mistretta C, Rowley H, Chen GH. Radiation dose reduction in time-resolved CT angiography using highly constrained back projection reconstruction. Phys Med Biol. 2009;54:4575–4593.
4. Becker HC, Augart D, Karpitschka M, Ulzheimer S, Bamberg F, Morhard D, Neumaier K, Graser A, Johnson T, Reiser M. Radiation exposure and image quality of normal computed tomography brain images acquired with automated and organ-based tube current modulation multiband filtering and iterative reconstruction. Invest Radiol. 2012 Mar;47:202–207.
5. Xia T, Alessio AM, De Man B, Manjeshwar R, Asma E, Kinahan PE. Ultra-low dose CT attenuation correction for PET/CT. Phys Med Biol. 2012;57:309–328.
6. Negi N, Yoshikawa T, Ohno Y, Somiya Y, Sekitani T, Sugihara N, Koyama H, Kanda T, Kanata N, Murakami T, Kawamitsu H, Sugimura K. Hepatic CT perfusion measurements: a feasibility study for radiation dose reduction using new image reconstruction method. Eur Radiol. 2012;81:3048–3054.
7. Tao Y, Chen GH, Hacker TA, Raval AN, Van Lysel MS, Speidel MA. Low dose dynamic CT myocardial perfusion imaging using a statistical iterative reconstruction method. Med Phys. 2014;41:0719141.
8. Wiedmann U, Neculaes VB, Harrison D, Asma E, Kinahan PE, De Man B. X-ray pulsing methods for reduced-dose computed tomography in PET/CT attenuation correction. Proc SPIE Med Imaging. 2014;9033:2Z.
9. Hussein E. Computed Radiation Imaging: Physics and Mathematics of Forward and Inverse Problems. Altham MA. Elsevier-USA; 2011.
10. Crawford CR, Kak AC. Aliasing artifacts in computerized tomography. 1st ed. Appl Opt. 1979;18:3704–3711.
11. Gentle DJ, Spyrou NM. Region of interest tomography in industrial applications. Nucl Instr Meth Phys Res. 1990;299: 534–537.
12. Truong TK, Wang LJ, Reed IS, Hsieh WS. Image data compression using cubic convolution spline interpolation. IEEE Trans Image Process. 2000;9:1988–1995.
13. Hong SH, Wang L, Truong TK, Lin TC, Wang LJ. Novel approaches to the parametric cubic-spline interpolation. IEEE Trans Image Process. 2013;22:1233–1241.
14. Keys RG. Cubic convolution interpolation for digital image processing. IEEE Trans Acoust Speech Signal Process. 1981;29:1153–1160.
15. So A, Hsieh J, Li JY, Hadway J, Kong HF, Lee TY. Quantitative myocardial perfusion measurement using CT perfusion: a validation study in a porcine model of reperfused acute myocardial infarction. Int J Cardiovasc Imaging. 2012;28:1237–1248.
16. Busono P, Hussein E. Algorithms for density and composition-discrimination imaging for fourth-generation CT systems. Phys Med Biol. 1999;44:1455–1477.
17. Branch KR. Incremental benefit of CT perfusion to CT coronary angiography: another step to the one-stop-shop? JACC Cardiovasc Imaging. 2019;12:350–352.
18. Lauzier PT, Tang J, Chen GH. Prior image constrained compressed sensing: implementation and performance evaluation. Med Phys. 2012;39:66–80.
19. Sidky EY, Kao CM, Pan X. Accurate image reconstruction from few-views and limited angle data in divergent-beam CT. J Xray Sci Technol. 2006;14:119–139.
20. Yazdanpanah AP, Regentova EE. Sparse-view CT reconstruction using curvelet and TV-based regularization. In: Campilho A., Karray F. (eds) Image Analysis and Recognition. 13th International Conference, ICIAR 2016 Proceedings, Portugal, July 13-15, 2016, Springer Cham.
21. Qi H, Chen Z, Guo J, Zhou L. Sparse-view computed tomography image reconstruction via a combination of L(1) and SL(0) regularization. Biomed Mater Eng. 2015;26 *Suppl* 1:S1389–98.
22. Huang J, Zhang Y, Ma J, Zeng D, Bian Z, Niu S, Feng Q, Liang Z, Chen W. Iterative image reconstruction for sparse-view CT using normal-dose image induced total variation prior. PLoS One. 2013;8(11):e79709.
23. Bertram M, Wiegert J, Schafer D, Aach T, Rose G. Directional view interpolation for compensation of sparse angular sampling in cone-beam CT. IEEE Trans Med Imaging. 2009;28(7):1011–22.
24. Zhang H and Sonke J-J. Directional sinogram interpolation for sparse angular acquisition in cone-beam computed tomography. J Xray Sci Technol. 2013;21:481–496.
25. Lee D, Choi S, Kim H. High quality imaging from sparsely sampled computed tomography data with deep learning and wavelet transform in various domains. Med Phys. 2019;46:104–115.
26. Enjilela E, Lee TY, Hsieh J, Wisenberg G, Teefy P, Yadegari A, Bagur R, Islam A, Branch K, So A. Ultra-low dose quantitative CT myocardial perfusion imaging with sparse-view dynamic acquisition and image reconstruction: a feasibility study. Int J Cardiol. 2018;254:272–281.